Recommendations for sonic boom community noise testing measurement and analysis FREE

Mark C. Anderson; Kent L. Gee ; J. Taggart Durrant; Alexandra Loubeau; William J. Doebler; Jacob Klos

Check for updates

View Online

Export Citation

07 August 2024 22:40:37

Proceedings of Meetings on Acoustics

183rd Meeting of the Acoustical Society of America

Nashville, Tennessee

5-9 December 2022

*Noise: Paper 2pNS5

Recommendations for sonic boom community noise testing measurement and analysis

Mark C. Anderson, Kent L. Gee and J. Taggart Durrant
Department of Physics and Astronomy, Brigham Young University, Provo, UT, 84602;
anderson.mark.az@gmail.com; kentgee@byu.edu; taggart.durrant@gmail.com

Alexandra Loubeau, William J. Doebler and Jacob Klos
Applied Acoustics Branch, NASA Langley Research Center, Hampton, VA, 23666; a.loubeau@nasa.gov;
william.j.doebler@nasa.gov; j.klos@nasa.gov

As part of its Quesst mission, NASA will fly the supersonic X-59 aircraft over communities to assess human annoyance to quieter sonic booms. As preparation for this flight test campaign continues, there are still many unanswered questions regarding best practices for sonic boom measurements inside and outside communities. This paper features sonic boom measurement and signal processing information including time-domain windowing, zero padding, digital pole-shift filtering, ground-based vs. elevated microphones, atmospheric turbulence, and contaminating noise mitigation. This work both summarizes previous recommendations and provides new recommendations for sonic boom measurement and signal processing. Thus, this paper serves as an overview of the research and recommendations.

*Young Presenter Award / Noise Technical Committee

07 August 2024 22:40:37

INTRODUCTION

As part of its Quesst mission, NASA will demonstrate quiet supersonic aircraft technology (NASA, 2024). This mission will feature a new aircraft, the X-59, that is designed to cruise at Mach 1.4 while producing a substantially quieter sonic boom, often referred to as a "low-boom", than previous aircraft (Loubeau and Page, 2018). To determine the human response to low booms, the X-59 will overfly several different communities across the USA, and local residents will fill out surveys indicating their level of annoyance to each event, similar to previous test campaigns (see Page *et al.*, 2014; Page *et al.*, 2020). These survey results will then be combined with acoustic data on the ground to determine a dose-response relationship (Lee *et al.*, 2020) that indicates a relationship between metric levels and human annoyance. The final results will then be delivered to regulators to inform decisions on the future of overland commercial supersonic flight.

Over the past several decades, numerous theoretical advancements have helped develop the theory required to design a low-boom aircraft like the X-59 (Maglieri *et al.,* 2014). For the X-59 tests, it is imperative to collect acoustic data that are both precise and accurate. One particular challenge is that the measurements of low booms are more susceptible to ambient and instrumentation noise contamination than classical, high-amplitude N-waves. Additionally, the sonic boom perception metrics of interest (see Loubeau and Page, 2018) are frequency-dependent and can be sensitive to contaminating noise and turbulence effects. These metrics, discussed in Loubeau and Page (2018) are the Perceived Level (PL) (Stevens, 1972; Shepherd and Sullivan, 1991), the Indoor Sonic Boom Annoyance Predictor (ISBAP), and the A-, B-, D-, and E-weighted sound exposure levels (SEL).

Brigham Young University (BYU) has been working with NASA to determine appropriate measurement and analysis techniques for sonic booms to help overcome some of these challenges. This paper summarizes prior research and newer analyses. The following topics are discussed in subsequent sections:

- Time-domain windowing
- Zero-padding prior to FFT analyses
- Digital pole-shift filtering
- Ground-based vs. elevated microphones
- Atmospheric turbulence
- Contaminating noise removal

1. WINDOWING

One of the many factors to consider when analyzing sonic boom recordings is time-domain windowing prior to performing a fast Fourier transform (FFT)-based spectral analysis. Windowing ensures that the waveform endpoints are set to zero, thereby reducing spectral leakage due to discontinuities at the waveform end points. One useful window choice is a Tukey (or tapered cosine) window because it leaves most of the waveform unaffected. The ramp portions of this window are defined by cosine functions, and the length of the ramp portions is defined by the "cosine fraction." This is illustrated in Figure 1. As an example, a cosine fraction of 0.4 indicates that each ramp individually covers 20% of the waveform, for a total of 40% of the waveform being tapered. Thus, the percentage of the waveform tapered by each individual ramp is determined by dividing the cosine fraction by two and multiplying by one hundred. In the limit that the cosine fraction becomes zero, the Tukey window becomes a rectangular window. In the limit that the cosine fraction becomes unity, the Tukey window becomes a Hann window. A cosine fraction of 0.1 is recommended for sonic boom analyses where waveforms start 100 ms before the peak of the primary shock and the total recording length is 650 ms, as shown in Figure 2(a) and (c). This recording length convention is the same as used in Page *et al.* (2014), though the lead time of 100 ms recommended here is shorter than in Page *et al.* (2014). This captures more of the post-boom noise if that is of interest to a particular analysis.

The choice of cosine fraction is relatively unimportant as long as the window is not too rectangular, and the ramps do not attenuate the main shocks. The effects of different cosine fractions on sonic boom metrics can be studied directly, as is shown in Figure 2. In this example, sonic boom metrics are calculated with varying cosine fractions. Figure 2(a) shows an example 650-ms boom recording from the NASA Carpet Determination in Entirety Measurements I (CarpetDIEM I) test campaign (Durrant *et al.,* 2022) along with a reference Tukey window using a cosine fraction of 0.1. Figure 2(b) shows the results of applying different cosine fractions and displays the results for each metric relative to a cosine fraction of 0.1, i.e., metric computed with a given cosine fraction minus metric computed with a 0.1 cosine fraction. This was done to visualize differences more easily

for each metric simultaneously. The same analysis is shown for another boom, from the NASA Quiet Supersonic Flights 2018 (QSF18) test campaign (Page *et al.,* 2020; Anderson *et al.*, 2022a), in Figure 2(c) and (d). The two examples are included to demonstrate that the results are similar for booms that have different relative amounts of post-boom noise. For both waveforms, the metric values all have a region of relative flatness between a cosine fraction of about 0.05 to 0.3. Divergences from this flat region at small cosine fractions are likely due to the window being too rectangular and causing waveform edge discontinuity, especially for the boom in Figure 2(c), which has notable post-boom noise and has a lower metric value, making it more sensitive to the discontinuity. This is because a nearly rectangular window will introduce broadband noise into the spectrum, increasing the metric value. Notice how for both booms, the metrics all diverge simultaneously at and above a cosine fraction of 0.3. For this particular cosine fraction, the individual ramp lengths are $0.3/2 \times 650$ ms $= 97.5$ ms, which means that the initial ramp will start reducing the primary shock amplitude. For waveforms with 100 ms of lead time before the peak of the primary shock and a total duration of 650 ms, a cosine fraction of 0.1 seems to be a suitable choice.
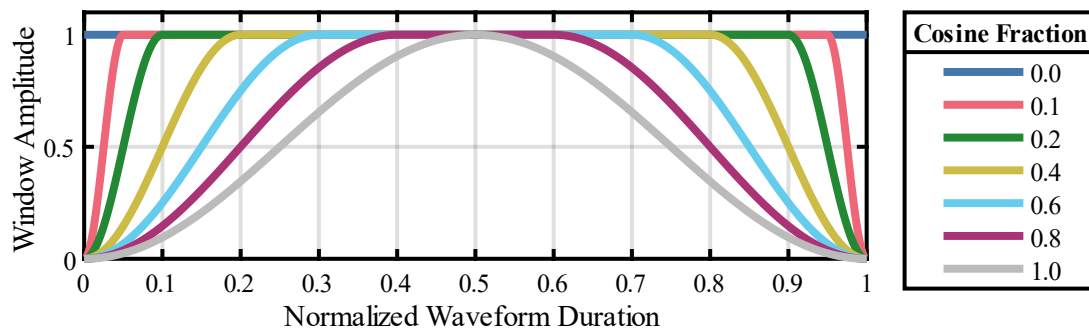

Figure 1. Several example Tukey windows, each with a different cosine fraction. A rectangular window is produced when the cosine fraction is zero, and a Hann window is produced by setting the cosine fraction to unity.

An asymmetric window may also be desirable, where the second ramp is longer than the first (Klos, 2022). This would enable an even more gradual taper to zero for the post-boom noise. This window type is analyzed in Figure 3. Part (a) shows the same boom as analyzed in Figure 2(c) and (d), but with an example asymmetric window superposed on top of the waveform. Part (b) shows the same type of analysis as Figure 2, but where the first ramp is kept at a cosine fraction of 0.1 (covering 5% of the recording) and only the second ramp cosine fraction is varied between 0–0.5 (0–25% of the recording). Evidently, increasing the second ramp length has marginal effects on the metric values, so long as its cosine fraction is greater than about 0.05 (2.5% of the recording). Therefore, an asymmetric window is also a good choice when analyzing sonic booms, though for this example it is not necessarily better than a symmetric window.

There likely exist other acceptable windows that could be successfully applied to sonic boom waveforms. Overall, the choice of window appears to be relatively unimportant so long as the primary boom is not affected by the windowing. In other words, the post-boom noise is a small contribution to the metric values, and a cosine fraction of 0.5 (25% of the recording) for the latter half of the waveform only has a 0.25 dB impact. This also implies that the window gain is negligible compared to the primary boom signal, which is not affected by the window. Further research could be performed to determine whether the claims in this section hold true for recordings with lower signal-to-noise ratios.
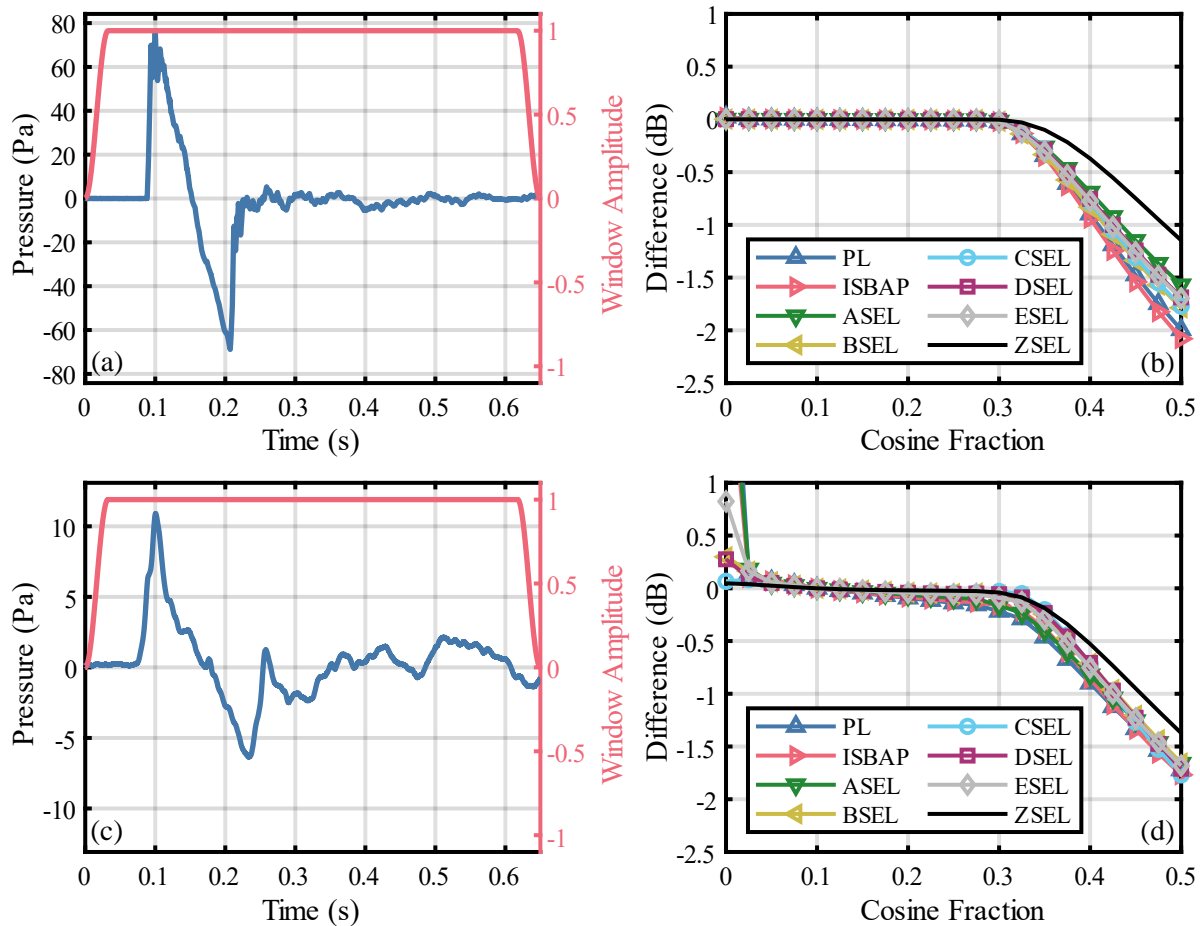
Figure 2. The effects of different cosine fractions on sonic boom perception metric values. (a) An example waveform from CarpetDIEM I along with a reference Tukey window with a cosine fraction of 0.1. (b) All sonic boom metrics shown relative to their calculated values with a cosine fraction of 0.1. (c) Similar to (a) but using a boom from QSF18 with notable post-boom noise. (d) Similar to (b) but using the QSF18 boom.
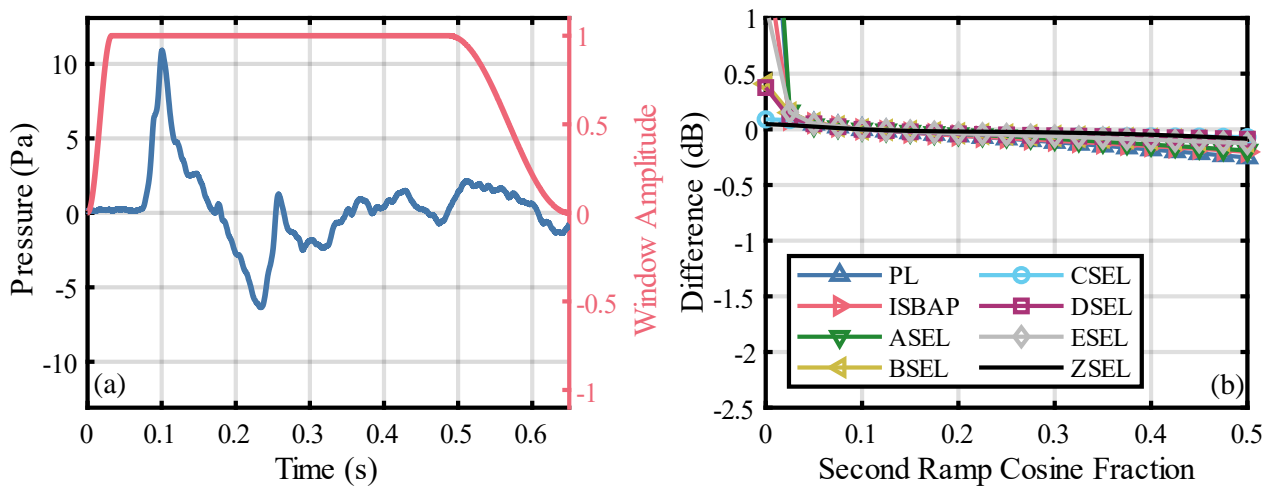

Figure 3. Analyzing an asymmetric window on the same boom as analyzed in Figure 2(c) and (d). (a) The boom is shown with an example window. The first ramp has a cosine fraction of 0.1 and the second ramp has a cosine fraction of 0.5, meaning it covers 25% of the recording. (b) The second ramp taper ratio is varied and the effects on the metrics are shown relative to the case where the taper ratio for the second ramp is equal to 0.1.

2. ZERO PADDING

When performing an FFT analysis over a short time interval, the frequency resolution is sparser than for a longer time interval. When converting the spectrum into one-third octave (OTO) bands, this sparse frequency resolution results in a nonphysical distribution of energy in adjacent OTO bands at low frequencies. An example is the spectrum shown in Figure 4(a). Notice the jagged peaks and troughs in the spectrum below 10 Hz. A solution to this issue is to use a longer recording to increase the frequency resolution and distribute a proper proportion of energy into each OTO band. For sonic boom recordings, this can be accomplished through zero padding. After windowing the signal, zeros are artificially appended (and/or prepended) onto the waveform, creating a longer recording. Because the sonic boom is a one-time impulse event, and many sonic boom metrics are exposure metrics, adding zeros to the signal does not affect those final metric values.

To determine the total duration of the padding required to remove the jagged peaks in the low-frequency spectrum, spectra of waveforms with increasing pad lengths were computed, and the results are shown in Figure 4(b). This analysis demonstrates that a pad of four seconds, resulting in a padded waveform of total duration 4.650 seconds, is a good choice to smooth the spectrum down to 1 Hz. Larger padding will always produce even smoother results but is more computationally time-consuming for FFT calculations. Therefore, we recommend applying up to four seconds of zero-padding to the windowed waveform before performing an FFT, if smooth FFT results are desired. An example is shown in Figure 5, where the four seconds of padding is split with two seconds before and two seconds after the windowed waveform. This could also be applied as four seconds either before or after the recording.
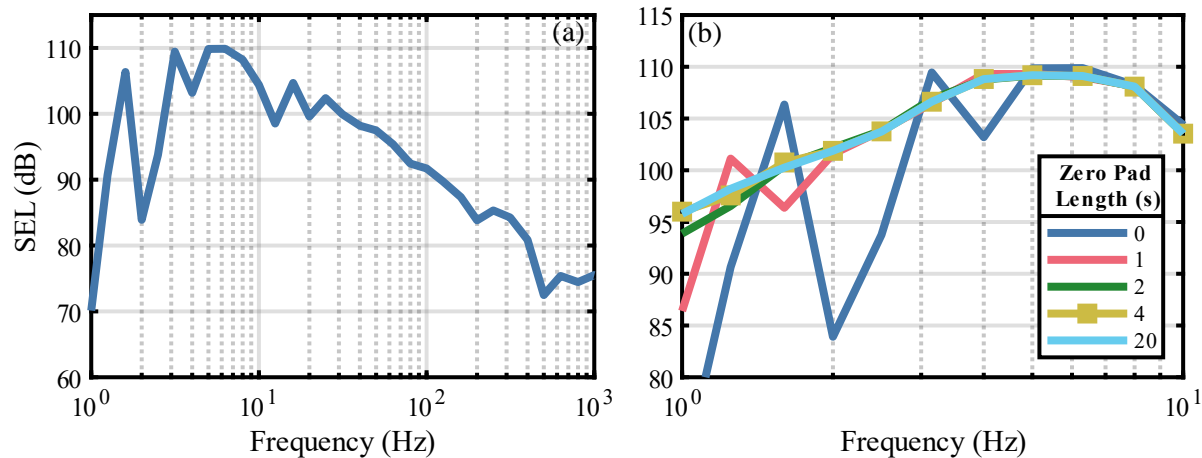

Figure 4. Effects of zero-padding. (a) The original OTO spectrum calculated using a 650-ms recording. Notice the jaggedness below 10 Hz. (b) Applying different pad amounts.
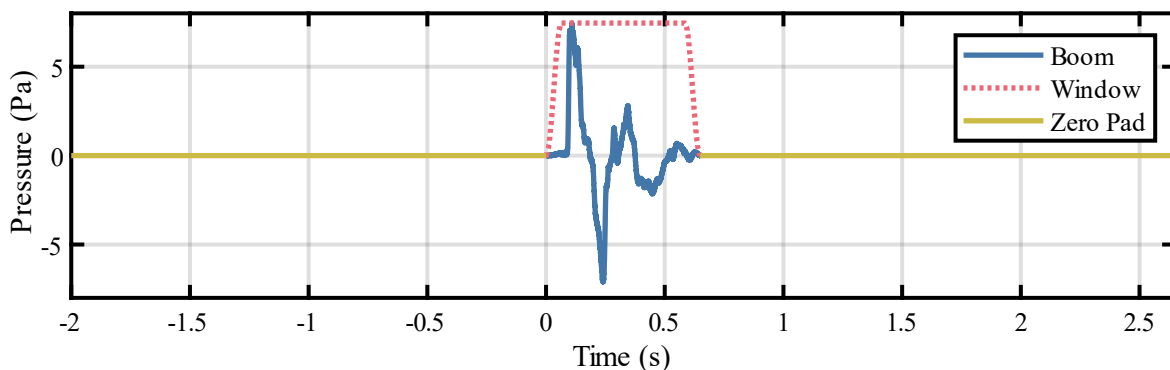

Figure 5. An example waveform with the recommended four seconds of zero padding applied to the recording. The pad is applied after windowing, the window height has been scaled to match the waveform amplitude, and the cosine fraction of the window has been increased to 0.2 for easier viewing.

3. DIGITAL POLE-SHIFT FILTERING

Another important choice when making sonic boom measurements is which microphone to use. Sonic booms can have substantial frequency content at low (< 10 Hz) and high (> 10 kHz) frequencies. Microphones capable of measuring lower frequencies tend to have low sensitivities and thus higher self-noise. This corrupts the high-frequency end of the spectrum and biases some sonic boom metric calculations. On the other hand, microphones with higher sensitivities, and thus lower self-noise, tend to fail to accurately represent the low-frequency end of the spectrum. This creates a dilemma – we can either use a high-noise microphone to capture the low frequencies properly, or we can use a low-noise microphone to capture the high frequencies properly. The low frequencies are important in accurately representing the waveform shape for comparison with theoretical models, but the higher frequencies are important in calculating the sonic boom metrics (Klos, 2022).

A solution to the problem of poor low-frequency response is to use digital pole-shift filtering (Rasband *et al.*, 2023; see also Marston, 2006). By shifting the microphone corner frequency to a lower value, this post-processing technique stably adjusts the magnitude and phase of the microphone low-frequency response to account for poor low-frequency performance of higher-sensitivity microphones. Thus, a high-sensitivity, low-self-noise microphone can be used, and the proper waveform shape can still be recovered, satisfying many of the needs of those interested in metrics and those interested in modeling. An example result is shown in Figure 6, which shows measurements of a boom at QSF18 measured with adjacent microphones (see Anderson *et al.*, 2022a). Part (a) shows the waveforms. The black curve shows a boom measured with a PCB 378A07 microphone, which represents the target waveform shape because it has the more accurate low-frequency response. A waveform was also measured with a GRAS 40AE microphone (red), a higher-sensitivity microphone with a frequency response that does not resolve the low frequencies. The corrected waveform (green) is the result of applying digital pole-shift filtering to the GRAS 40AE-measured waveform via the methods discussed in Rasband *et al.* (2023). Part (a) demonstrates that the corrected waveform is now in much better visual agreement with the PCB 378A07 measurement. Notice from parts (b) and (c) that the corrected result now maintains its lower electrical noise floor at higher frequencies while more accurately capturing the low-frequency content. In short, digital pole-shift filtering can enable accurate waveform representation while still providing low-noise measurements. Customized filters can be applied to better optimize particular hardware configurations, as discussed in Rasband *et al.* (2023).
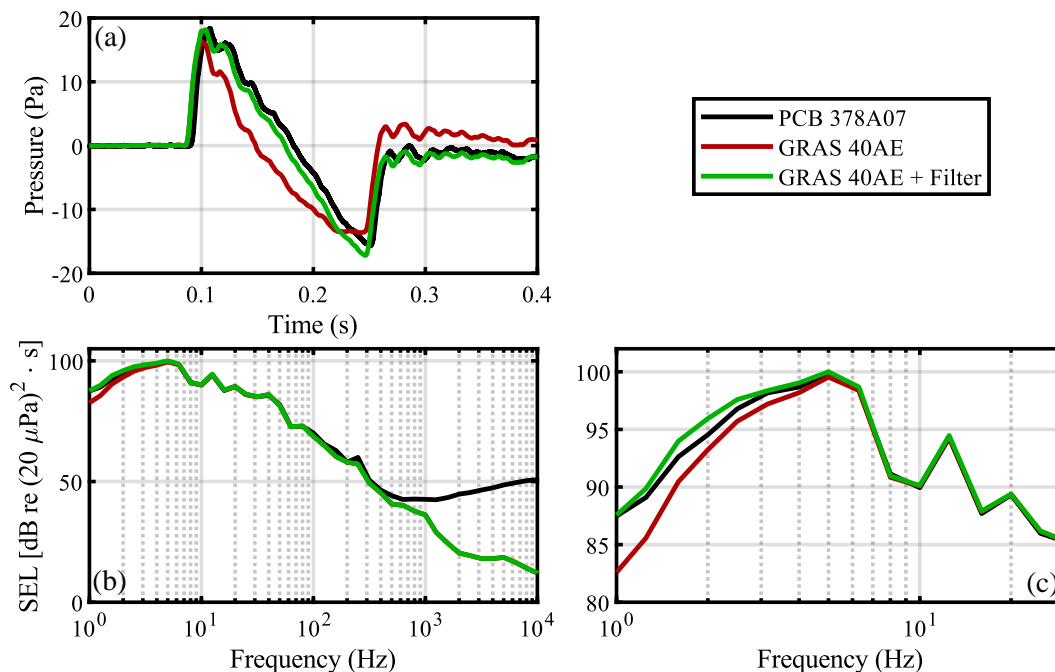

Figure 6. Applying digital pole-shift filtering to a measured sonic boom. (a) The GRAS 40AE measurement can be corrected at low frequencies via digital pole-shift filtering to capture the true waveform shape more accurately. (b) Spectra from 1 Hz – 10 kHz. Although the PCB 378A07 recording captures the overall waveform shape the best, it has a much higher noise floor than the GRAS 40AE recording. (c) The low-frequency effects of applying the digital pole-shift filter.

4. GROUND-BASED VS. ELEVATED MICROPHONES

Elevated microphones have been used in the past as a means of weatherproofing a microphone against water damage (Page *et al.,* 2020; Anderson *et al.*, 2022a). However, elevated microphones are subject to multipath interference at frequencies that are important to sonic boom metrics, as discussed in a recent article by researchers at Volpe Transportation Research Center, BYU, and NASA Langley Research Center (Downs *et al.*, 2022). Some interesting data are shown below that supplement results published by Gee *et al.* (2020), Downs *et al.* (2022), Anderson *et al.* (2022a), and Durrant *et al.* (2022). The interested reader is referred to those publications for a more thorough treatment of elevated microphones in sonic boom measurements.

Figure 7 shows a comparative microphone station at CarpetDIEM I (Durrant *et al.*, 2022). Three of the channels (with the same type of microphone) are used to produce the results in Figure 8. The three configurations are COUGAR (see Anderson *et al.*, 2022b), Ground-Board, and Elevated. Further details on these types of configurations are found in Anderson *et al.* (2022a). Figure 8(a) shows the measured spectra of the three configurations for the same sonic boom. Figure 8(b) shows the difference between the mean spectra and the COUGAR configuration over the entire measurement campaign of 22 booms for this location. Notice the strong spectral nulls seen at 400 Hz, 1.25 kHz, and 2 kHz for the Elevated microphone. Figure 8(c) shows the loudness spectra in sones for each configuration for the same boom as part (a). Lastly, Figure 8(d) shows the mean loudness spectra over the entire measurement campaign. To better visualize the effects of the Elevated microphone on the mean loudness spectrum, part (d) shows the absolute spectra rather than the relative spectra. The overall loudness reduction effect of elevating a microphone is evident in the reduced spectral levels between 100 and 1000 Hz in the loudness spectra. For the averaged loudness spectra in (d), the COUGAR PL is 101.8 dB, the Ground-Board PL is 102.1 dB, and the Elevated PL is 100.1 dB, meaning that the Elevated setup averaged about 2 dB less for the PL metric than the other two configurations.

Figure 7. Comparative station at CarpetDIEM I. (Top Left) a Ground-Board configuration. (Top Right) An Elevated configuration, with the microphone raised 18 inches (46 cm) above the ground. (Bottom) Two COUGAR configurations with different microphones. The Ground-Board, Elevated, and COUGAR configurations compared in this paper all use a PCB 378A07 microphone. This station is referred to as PUMA 1 in Durrant et al. (2022).
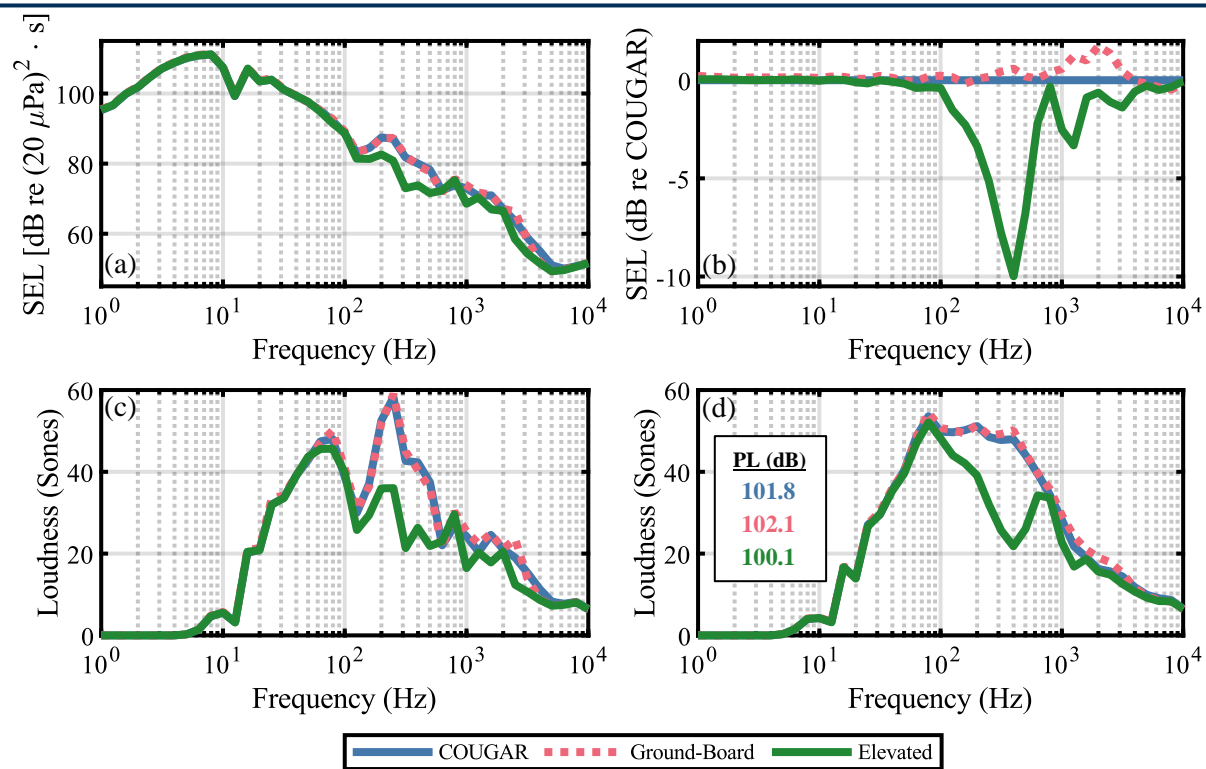
Figure 8. Comparison of three different microphone configurations at one location during CarpetDIEM I. (a) Spectra for each channel during a single boom event. (b) Twenty-two measurement mean spectra relative to COUGAR measurements at this location. (c) The loudness spectra for each channel during the same single boom event as part (a). (d) Twenty-two-measurement mean loudness spectra at this station.

5. ATMOSPHERIC TURBULENCE

Meteorological effects on sonic boom measurements have been studied for decades (Maglieri *et al.*, 2014). Of particular interest is the lowest portion of the atmosphere, known as the atmospheric boundary layer, where turbulence can be much greater than at higher altitudes. Turbulence may cause sonic boom waveforms measured over short distances to vary dramatically. To investigate turbulence effects on sonic booms further, BYU fielded a seven-microphone 400-ft (120-m) linear turbulence array directly under the flight track at CarpetDIEM (Durrant *et al.*, 2022). The array was oriented perpendicular to the flight track. Figure 9 shows the sonic boom from a single flyover measured at all seven microphones along the array. Notice the large visual differences between the waveforms across the array due to turbulence.

These differences translate into sonic boom metric variability, as indicated in Figure 10(a) for the PL metric. This includes booms from three supersonic overflights (A, B, and C). Each overflight is unique and shows different amounts of variability across the array. When considering the mean metric value for a boom, the confidence interval on that mean value varies with the amount of scatter. For example, Boom A has a narrower confidence interval width than Boom B. Figure 10(b) illustrates this for each metric. The metrics across the array for twelve booms at this station were calculated and the confidence interval (CI) half-widths for each metric for each boom were also calculated. The results can be interpreted as follows: the PL 90% confidence interval half-width (i.e., mean ± CI/2) was sometimes as narrow as 0.6 dB, but sometimes as wide as 2.7 dB. These results can be compared with those shown by Doebler (2017), where favorable agreement is found between the two. While these results are all for N-waves, these methods may be useful when studying measurements of low booms. It is therefore recommended that during X-59 testing, similar results be obtained by using multiple microphones at a single location to experimentally determine the variability due to atmospheric turbulence.
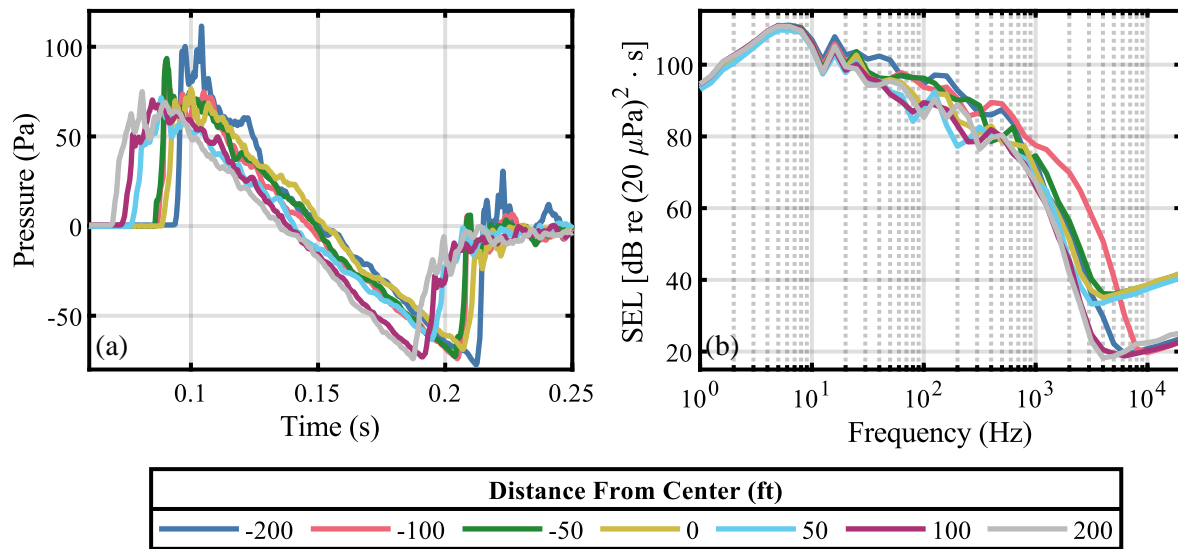
Figure 9. (a) Example waveforms measured across the turbulence array for a single boom event. (b) Corresponding spectra for the booms shown in part (a).
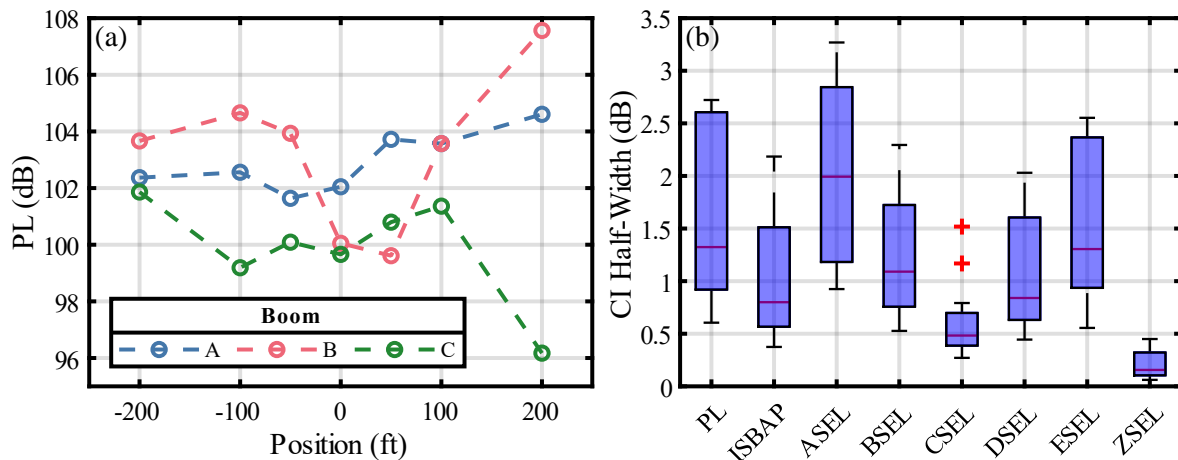

Figure 10. The effects of atmospheric turbulence on sonic boom metrics. (a) The PL metric for three example overflights varies widely across the array and each boom is unique. (b) Each overflight (N=12) has a unique confidence interval half-width for each metric mean value. Twelve overflights each with 7 boom measurements were used to calculate 90% confidence interval half-widths for each boom for each metric, and the results are shown as a box and whisker plot with the medians shown by a horizontal line. Red plus signs indicate outliers, and the red bars indicate the median values.

6. CONTAMINATING NOISE REMOVAL

One of the important problems continuing to face outdoor sonic boom measurements is the local ambient and instrumentation noise (Page *et al.*, 2014; Klos, 2020; Anderson *et al.*, 2021; Klos, 2022; Anderson *et al.*, 2024). Noise can artificially inflate metric values, resulting in an overall bias error in sonic boom metric distributions. To compute accurate sonic boom metrics, this problem must be dealt with effectively.

The following method is proposed for removal of ambient and instrumentation noise (hereafter considered together under the term "contaminating noise") from sonic boom recordings:

1. Record 650-ms of contaminating noise before the boom, as well as a 650-ms recording containing the boom.
2. Calculate the contaminating noise and the boom spectra, then subtract them to calculate the signal-to-noise ratio (SNR) spectrum.

3. Determine the first OTO band center frequency at which the SNR becomes less than 3 dB. This becomes the filter cutoff or corner frequency.

4. Apply either a sixth-order Butterworth-magnitude filter (time domain) or a brick-wall filter (frequency domain) with the determined cutoff frequency from the previous step. For the brick-wall filter, the spectral data at the cutoff frequency are kept, and data at frequencies greater than the cutoff frequency are removed. Note that the Butterworth filter can be applied as two third-order magnitude filters (one forward and one backward) to produce a usable waveform with zero phase distortion. This can be done in MATLAB® r2022a via the *filtfilt* command.

5. Calculate metrics using the filtered data.

To demonstrate the success of this filtering approach, a detailed example is included in this paper. For this example, we use a simulated NASA C609 low boom (Rallabhandi and Loubeau, 2022) and real-world contaminating noise recorded during QSF18. The simulated waveform is shown Figure 11(a) and is referred to as the "Clean Boom". The metrics calculated using this waveform are considered true because there is no contaminating noise. In Figure 11(b), 1300 ms of continuous contaminating noise has been superposed on the clean boom, with 650 ms occurring before the boom recording. The new 1300-ms recording is then split into the "Preboom Contaminating Noise" and the "Mock Recording".
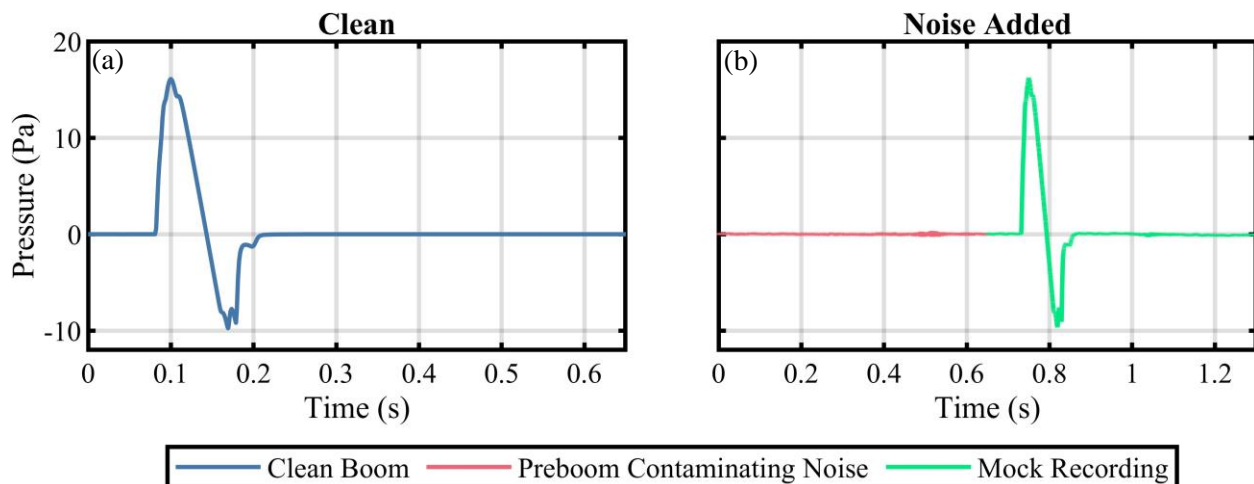

Figure 11. (a) A simulated low boom, known as the clean boom. (b) A total of 1300 ms of contaminating noise has been superposed on the clean boom, with 650 ms being placed before the start of the boom portion of the recording. The new waveform is 1300 ms in duration and can be split into a preboom contaminating noise phase and a mock recording phase.

The spectra for these waveforms are shown in Figure 12(a). Notice that the boom spectrum is dominant at low frequencies, and the contaminating noise spectrum is dominant at frequencies greater than a few hundred Hertz. Although there is sometimes contaminating noise due to wind, such effects tend to be at frequencies low enough to have a relatively minor effect on sonic boom metrics. Notice also that the contaminating noise is not stationary, causing the preboom ambient and mock recording spectra not to match perfectly at high frequencies. This effect can also be seen in Figure 12(b), which shows the SNR spectrum of the mock recording relative to the preboom contaminating noise. This nonstationarity is the reason that a purely spectral-subtraction-based method for contaminating noise removal was avoided when developing this method. Experience tends to show that although the contaminating noise is nonstationary, the method presented in this paper tends to perform well.
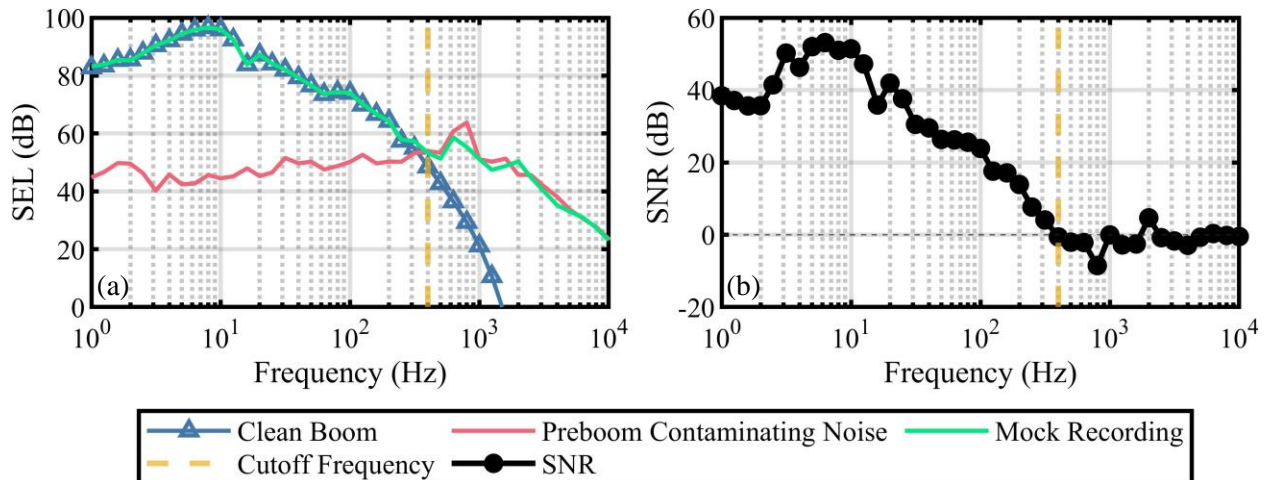
Figure 12. Determining the cutoff frequency. (a) The three spectra are plotted together. (b) The SNR between the Mock Recording and the Preboom Contaminating Noise is plotted.

What do the spectra look like after the filtering has been applied? Figure 13 contains the filtered mock recording results. Parts (a) and (b) show the flat-weighted spectral results for both the Butterworth and brick wall methods respectively. Parts (c) and (d) show the loudness spectra obtained as part of the PL metric calculation. For this example, the clean boom had a PL of 76.1 dB and the mock recording had a PL of 80.1 dB. The Butterworth filter brought the PL down to 76.0 dB and the Brick wall filter brought the PL down to 75.9 dB. Notice that both types of filters work well and returned the PL to within 0.2 dB of the clean case. Note also that because the brick wall filter performed similarly to the Butterworth filter, we can conclude that attempts to match the high-frequency spectral slope of the clean boom more closely are unlikely to yield large improvements. It is also important to note that this method, like other methods such as the methods proposed by Klos (2022), relies on the assumption that the contaminating noise is stationary. Additional limitations of the methods proposed in this paper are that tonal noise can cause the filter cutoff frequency to be set to an unnecessarily low frequency and that results are limited to low-pass filtering.

How does this approach compare to another state-of-the-art technique? Klos (2022) proposed an adaptation of ISO 11204 (ISO11204:2010, 2010) that allows for more aggressive corrections than typically afforded by that standard. The most successful of the proposed adaptations are denoted "Custom E" and "Custom F". To make a direct comparison, a set of 300 simulated C609 low booms were randomly paired with contaminating noise recordings from QSF18. The differences between the filtered mock recording PL values and the clean boom PL values were calculated and are shown as histograms in Figure 14. Part (a) shows only the results using the ISO 11204 adaptations. Part (b) superimposes the results from the methods proposed in this paper. All four methods successfully remove the contaminating noise for the PL metric. These methods should all continue to be studied once real low-boom measurements are available. It is possible that multiple methods ought to be used in tandem because they are likely robust to different types of errors.

Further details on the methods proposed within this paper have been recently published in the Journal of the Acoustical Society of America (Anderson *et al.*, 2024).
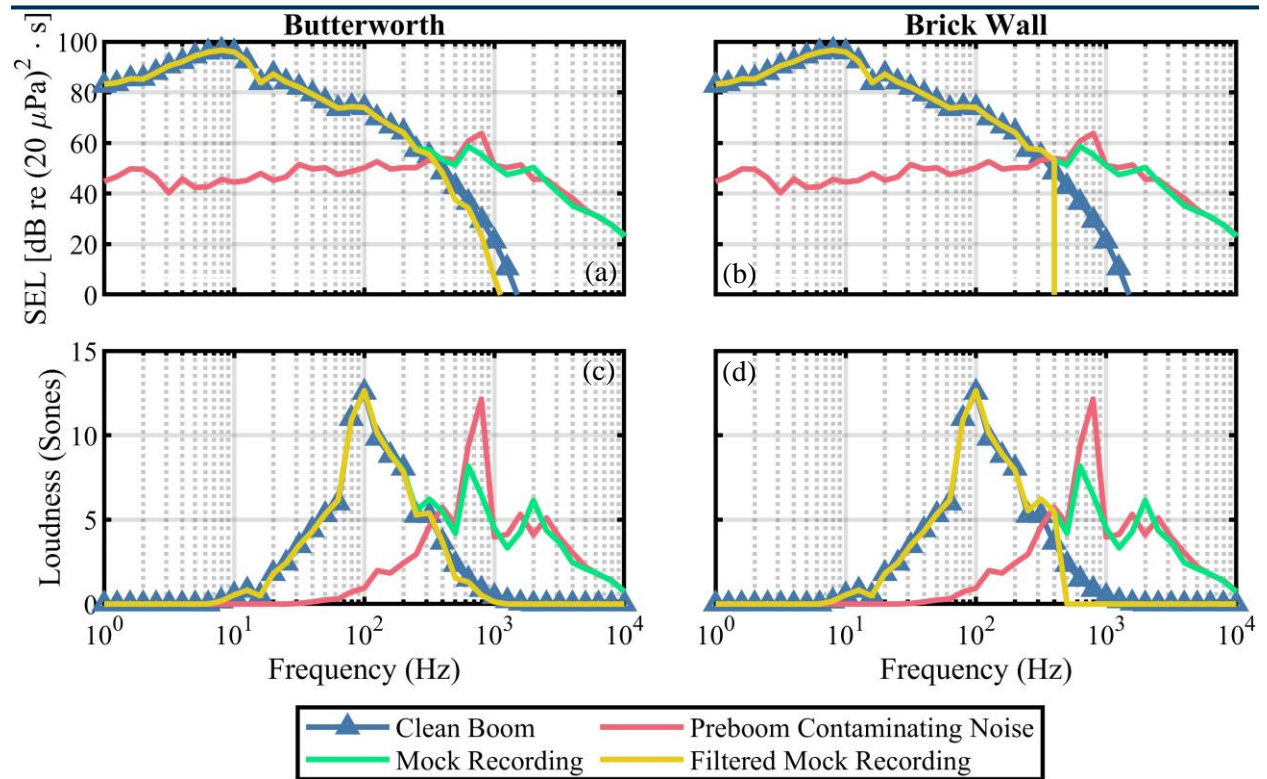
Figure 13. Applying the filters to the data: (a) the flat-weighted spectra using the Butterworth filter, (b) the flat-weighted spectra using the brick wall filter, (c) the loudness spectra using the Butterworth filter, and (d) the loudness spectra using the brick wall filter.
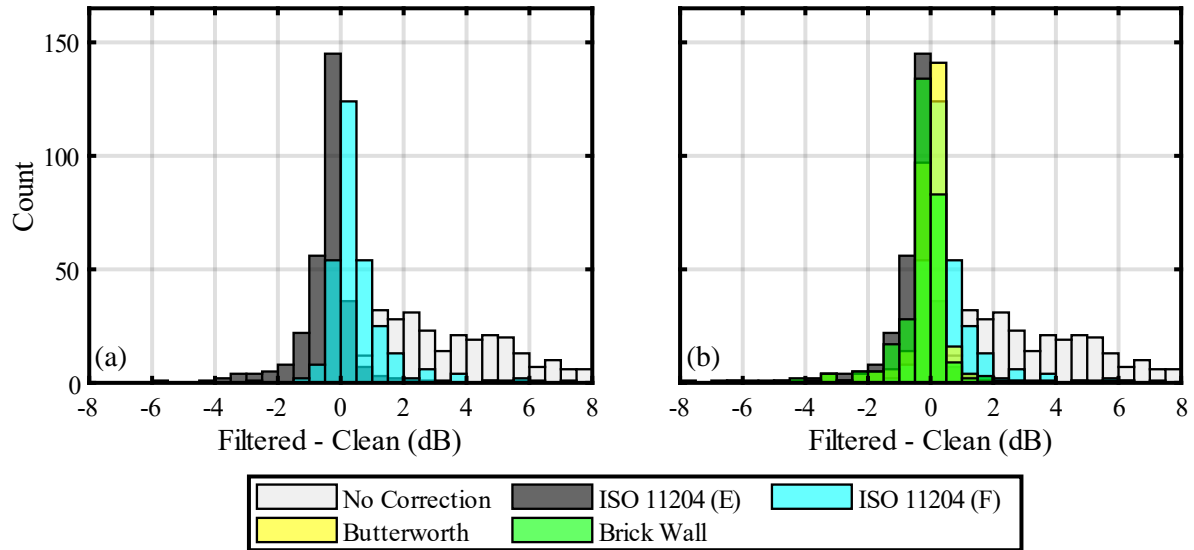

Figure 14. Comparison with the method proposed in Klos (2022): (a) the distribution of filtered metrics relative to the clean boom and (b) the same distributions, but with the filtering methods proposed in this paper included. Note that the "No Correction" case extends beyond the plot limits up to a maximum value of +20.6 dB.

7. SUMMARY OF RECOMMENDATIONS

The methods outlined and summarized in this paper have primarily focused on how to make accurate sonic boom measurements and how to process the recordings to obtain high-fidelity results. This research has spanned several topics, and the current recommendations are given in this paper. In summary, we recommend:

- Use a Tukey (tapered-cosine) window for time-domain windowing prior to an FFT analysis. Ensure that the taper does not impact the primary shock.
- Use up to four seconds of zero padding for smooth spectra down to 1 Hz when performing an FFT-based OTO spectral analysis and the recording length is 650 ms.
- Use a high-sensitivity microphone that will accurately capture the higher frequencies. To restore the low-frequency content, apply digital pole-shift filtering.
- Use weather-robust ground-based microphones instead of elevated microphones.
- Use multiple microphones at a recording station during X-59 measurements to experimentally determine variability due to atmospheric turbulence.
- Use a sixth-order Butterworth magnitude filter to remove ambient and instrumentation noise from recordings. Alternatively, a frequency-domain brick wall filter may also be used, or those methods proposed by Klos (2022). These methods should all be used in tandem to produce error bars on final results.

Further recommendations regarding these topics can be found in the references included herein as well as within a forthcoming NASA contractor report (Gee et al., 2024).

ACKNOWLEDGEMENTS

REFERENCES

Anderson, M. C., Gee, K. L., Durrant, J. T., Loubeau, A., Doebler, W. J., **(2021)** "Investigating the impact of ambient noise on candidate sonic boom metrics," J. Acoust. Soc. Am. 150, A259-A259 https://doi.org/10.1121/10.0008214

Anderson, M. C., Gee, K. L., Novakovich, D. J., Rasband, R. D., Mathews, L. T., Durrant, J. T., Leete, K. M., and Loubeau, A. **(2022a)**. "High-fidelity sonic boom measurements using weather-robust measurement equipment," Proc. Mtgs. Acoust. 39, 040005. https://doi.org/10.1121/2.0001578

Anderson, M. C., Gee, K. L., Novakovich, D. J., Mathews, L. T., Jones, Z. T., **(2022b)** "Comparing two weather-robust microphone configurations for outdoor measurements," Proc. Mtgs. Acoust. 42, 040005 https://doi.org/10.1121/2.0001561

Anderson, M. C., Gee, K. L., Durrant, J. T., Loubeau, A., Doebler, W. J., Klos, J. **(2024)**, "Reducing contaminating noise effects when calculating low-boom loudness levels," J. Acoust. Soc. Am. **155**, 3889-3899 (2024) https://doi.org/10.1121/10.0026436

Doebler, W. J., **(2017)** "The minimum number of ground measurements required for narrow sonic boom metric 90% confidence intervals," M.S. Thesis at The Pennsylvania State University Graduate Program in Acoustics https://etda.libraries.psu.edu/catalog/14826wfd5057

Downs, R., Page, J., Durrant, J. T., Gee, K. L., Novakovich, D. J., Anderson, M. C., Loubeau, A., **(2022)** "Sonic boom measurements: Practical implications considering ground effects, microphone installation, and weather hardening", JASA Express Lett. 2, 104001 https://doi.org/10.1121/10.0014414

Durrant, J. T., Gee, K. L., Anderson, M. C., Mathews, L. T., Rasband, R. D., Novakovich, D. J., Loubeau, A., and Doebler, W. J. **(2022)**. "An overview of Brigham Young University's participation in NASA's CarpetDIEM campaign," Proc. Mtgs. Acoust. 43, 045002 https://doi.org/10.1121/2.0001589

Gee, K. L., Novakovich, D. J., Mathews, L. T., Anderson, M. C., and Rasband, R. D. **(2020)**. "Development of a weather-robust ground-based system for sonic boom measurements," NASA/CR-2020-5001870 (NASA Langley Research Center, Hampton, VA).

Gee, K. L., Anderson, M. C., Durrant, J. T., Blaine, J. D., Nyborg, K., Sorrell, A. K. **(2024)**. "Sonic Boom Analyses in Support of Improved X-59 Community Noise Testing," NASA Contractor Report (Publication Pending)

ISO11204:2010, "Acoustics — Noise emitted by machinery and equipment — Determination of emission sound pressure levels at a work station and at other specified positions in an essentially free field over a reflecting plane with negligible environmental corrections," **(2010)**

Klos, J. **(2020)** "Recommendations for Using Noise Monitors to Estimate Noise Exposure During X-59 Community Tests." NASA/TM–20205007926

Klos, J., **(2022)** "An Adaptation of ISO 11204 using Customized Correction Grades to Mitigate Ambient Noise Effects when Computing Sonic Boom Loudness Levels." NASA/TM-20220010779

Lee, J., Rathsam, J., Wilson, A., **(2020)** "Bayesian statistical models for community annoyance survey data," J. Acoust. Soc. Am. 147, 2222-2234 https://doi.org/10.1121/10.0001021

Loubeau, A. and Page, J., **(2018)** "Human perception of sonic booms from supersonic aircraft." Acoustics Today, 14(3): 23-30.

Maglieri, D. J., Bobbitt, P. J., Plotkin, K. J., Shepherd, K. P., Coen, P. G, Richwine, D. M, **(2014)** "Sonic Boom: Six Decades of Research," NASA/SP-2014-622.

Marston, T. M., **(2006)** "Diffraction correction and low-frequency response extension for condenser microphones," M.S. Thesis at The Pennsylvania State University Graduate Program in Acoustics

NASA, Quesst Mission Webpage, NASA, **(2024)**; nasa.gov/quesst.

Page, J. A., Hodgdon, K. K., Krecker, P., Cowart, R., Hobbs, C., Wilmer, C., Koening, C., Holmes, T., Gaugler, T., Shumway, D. L., Rosenberger, J. L., Philips, D., **(2014)** "Waveforms and Sonic Boom Perception and Response (WSPR): Low-Boom Community Response Program Pilot Test Design, Execution, and Analysis," NASA/CR–2014-218180

Page, J. A., Hodgdon, K. K., Hunte, R. P., Davis, D. E., Gaugler, T. A., Downs, R., Cowart, R. A., Maglieri, D. J., Hobbs, C., Baker, G., Collmar, M., Bradley, K. A., Sonak, B., Crom, D., Cutler, C., **(2020)** "Quiet Supersonic Flights 2018 (QSF18) Test: Galveston, Texas Risk Reduction for Future Community Testing with a Low-Boom Flight Demonstration Vehicle," NASA/CR–2020-220589

Rasband, R. D., Gee, K. L., Gabrielson, T. B., and Loubeau, A. **(2023)**. "Improving low-frequency response of sonic boom measurements through digital filtering," JASA Express Lett. **3**, https://doi.org/10.1121/10.0016751

S. K. Rallabhandi, A. Loubeau, "Summary of Propagation Cases of the Third AIAA Sonic Boom Prediction Workshop," Journal of Aircraft **59**(3), 578-694 (2022) https://doi.org/10.2514/1.C036327

Shepherd, K. P., Sullivan, B. M., **(1991)** "A Loudness Calculation Procedure Applied to Shaped Sonic Booms," NASA Technical Paper 3134

S. S. Stevens, "Perceived Level of Noise by Mark VII and Decibels (E)," J. Acoust. Soc. America (**51**) (2B), 575-601 **(1972)** https://doi.org/10.1121/1.1912880

07 August 2024 22:40:37